Dynamical study of D^*DK and $D^*D\bar{D}$ systems at quark level

Yue Tan[*]
Department of Physics, Yancheng Institute of Technology, Yancheng 224000, People's Republic of China

Xuejie Liu[†]
School of Physics, Henan Normal University, Xinxiang 453007, People's Republic of China

Xiaoyun Chen[‡]
College of Science, Jinling Institute of Technology, Nanjing 211169, People's Republic of China

Youchang Yang[§]
Department of Physics, Guizhou University of Engineering Science, Bijie 551700, People's Republic of China

Hongxia Huang[‖] and Jialun Ping[¶]
Department of Physics, Nanjing Normal University, Nanjing 210023, People's Republic of China

(Received 13 April 2024; accepted 10 June 2024; published 9 July 2024)

Inspired by the recent report from the LHCb Collaboration on T_{cc}, which can be interpreted as a molecular DD^*, we investigated two trimeson systems of the T_{cc} partner with $IJ^P = 01^-$ in the framework of a chiral quark model. In the first case, because of the attraction between D^* and $\bar{D}$, we explored the existence of bound states in the system $D^*D\bar{D}$, which is obtained by adding $\bar{D}$ into the molecular bound state T_{cc} (DD^*). Similarly, in the second case, we explored whether there is a bound state in the D^*DK system, which is obtained by adding K into the T_{cc}, given the attraction between D and K. The results show that both of them are bound states, in which the binding energy of the molecular state DD^*K is relatively small, only 0.4 ± 0.4 MeV, while the binding energy of $DD^*\bar{D}$ is up to 1.6 ± 0.3 MeV. According to the calculation results of the root-square-mean distances, the spatial structure of the two systems shows the obvious (DD^*)-$(\bar{D}/K)$ structure, in which D is close to D^* while DD^* as a whole is relatively distant from the third hadron $(\bar{D}/K)$, which are similar to the nucleon-electron structure. As a result, we strongly recommend that these bound states $DD^*\bar{D}$ and DD^*K are searched for experimentally.

DOI: 10.1103/PhysRevD.110.016005

I. INTRODUCTION

The quark model has been an important tool for understanding the low energy region of QCD; thus, unveiling the internal quark structure of hadrons is very important. At first, due to the limitation of experimental precision, the mesons found in experiments are mainly ground states, which can be well explained by the $q\bar{q}$ $(q = u, d, s, c, b)$ structure. However, the discovery of the $X(3872)$ opened a new era in the quark model [1]. Since the energy of the $q\bar{q}$ structure is 50–100 MeV in the quark model higher than the experimental value of $X(3872)$, the $q\bar{q}$ structure cannot explain the $X(3872)$ observed in experiments [2]. Therefore, the authors [3,4] proposed that the $X(3872)$ may not be a $q\bar{q}$ structure but rather a molecular state of $c\bar{q} - q\bar{c}$, specifically $D^*\bar{D}$, which has been confirmed by numerous studies. After that, excited heavy mesons near thresholds are widely believed to contain significant hidden-heavy molecular components $q\bar{q}' + n\bar{n}$ $(n = u, d, s)$ [5–8]. Until the recent discovery of T_{cc} [9], the view has been changed to the multiquark system that can be composed of open charm or bottom quarks, because the internal quark configuration of T_{cc} is a $c\bar{q}c\bar{q}$ configuration different from the previous view. Therefore, it is reasonable

[*]Contact author: tanyue@ycit.edu.cn
[†]Contact author: 1830592517@qq.com
[‡]Contact author: xychen@jit.edu.cn
[§]Contact author: yangyc@gues.edu.cn
[‖]Contact author: hxhuang@njnu.edu.cn
[¶]Contact author: jlping@njnu.edu.cn

to believe that with the continuous improvement of experimental accuracy in the future, the exotic states with an open flavor three-meson structure ($q\bar{q}' - q\bar{q}' - q\bar{q}'$) will be observed experimentally.

In fact, a lot of work [10–19] has been done on the calculation of the trihadron system. In 2015, the authors [10] take advantage of Faddeev-type Alt-Grassberger-Sandhas equations, in which two phenomenological and one chirally motivated $\bar{K}N$ potentials are used, to perform dynamically exact calculations of a quasibound state in the $\bar{K}\bar{K}N$ trihadron system. The result shows that $\bar{K}N$ is a good candidate of $\Lambda(1405)$, and $\bar{K}\bar{K}N$ is a good candidate of the $\Xi(1950)$ state. Based on the fact that mesons D and K can form $D_{s0}^*(2317)$, in Ref. [11], the authors search for bound states in the DDK system. By coupling effects, they found a bound state with the binding energy of the DDK system about 60–70 MeV. According to this result, Ref. [12] applies the Gaussian expansion method to study the $DDDK$ system and show that it binds as well. Through the study of the partial decay of DDK, the authors in Ref. [13] also believe that DDK is a stable state. In the framework of the effective Lagrangian approach, the authors of Ref. [14] claim that the molecular state $\bar{D}\bar{D}^*$ is a possible candidate for T_{cc}, while the molecular state $\bar{D}^{(*)}\Sigma_c$ is a candidate for P_c states. For the reason the two molecules share a meson $\bar{D}$, the trihadron state $\bar{D}\bar{D}^*\Sigma_c$ is also a possible stable state. The authors [15] further investigate three-hadron systems $\eta K^*\bar{K}^*$, $\pi K^*\bar{K}^*$, and $KK^*\bar{K}^*$ within the framework of fixed-center approximation, where $K^*\bar{K}^*$ is treated as the fixed center, corresponding to the possible scalar meson $a_0(1780)$ or the tensor meson $f_2'(1525)$. They find several resonances with a mass about 2000 MeV. Under the assumption that the heavy partner of the T_{cc} exists as a DD^* state, Ortega [16] explores the Efimov effect in the $D^*D^*D^*$ system and finds a stable bound state.

According to the above work, there may be stable bound states in the trihadron system, which is characterized by one of the meson pair forming exotic states reported by experiment. However, the three hadronic bound states obtained by these works are almost all at the hadronic level. To search for the stable trihadron state of the T_{cc} partner, we will deeply study the $DD^*\bar{D}$ system that is obtained by combining DD^* in T_{cc} and $D^*\bar{D}$ in $X(3872)$, as well as the DD^*K system that is obtained by combining DD^* in T_{cc} and DK in $D_{s0}^*(2317)$ within the quark level. In this article, the $S-D$ coupling effect is taken into account in the calculation to replace the contribution from the color structure of the three-meson structure. To calculate the hexaquark properties, we use the Rayleigh-Ritz variational method with a Gaussian expansion method (GEM), which allows us to expand each relative motion in the system in terms of Gaussian basis functions.

The structure of this paper is organized as follows: After the Introduction, details of the chiral quark model (ChQM) and GEM are introduced in Sec. II. In Sec. III, we present the numerical results and a method of finding. The last section is devoted to the summary.

II. THEORETICAL FRAMEWORK

Phenomenological models remain primary tools in unveiling the nature of experimentally observed multiquark candidates. Therefore, the D^*DK and $D^*D\bar{D}$ systems are thoroughly investigated by means of a ChQM. Furthermore, the GEM, renowned for its high accuracy in computing few-body systems, is utilized to explore the bound states of the hexaquark system.

A. Chiral quark model

In the ChQM, the Hamiltonian consists of three parts: the mass term (m_i), the kinetic term ($\frac{\vec{p}_i}{2m_i}$), and the potential term [$V(\mathbf{r}_{ij})$], which can be written as

$$H = \sum_{i=1}^{6} m_i + \frac{\vec{p}_{12}^2}{2\mu_{12}} + \frac{\vec{p}_{34}^2}{2\mu_{34}} + \frac{\vec{p}_{56}^2}{2\mu_{56}} + \frac{\vec{p}_{12,34}^2}{2\mu_{12,34}} + \frac{\vec{p}_{1234,56}^2}{2\mu_{1234,56}} + \sum_{i<j=1}^{6} [V_{\rm con}(\mathbf{r}_{ij}) + V_{\rm oge}(\mathbf{r}_{ij}) + V_{\chi,\chi=\pi,\eta,K,\sigma}(\mathbf{r}_{ij})], \quad (1)$$

where μ_{ij} and $\vec{p}_{ij}$ are the reduced mass and momentum of two interacting quarks or quark clusters, m_i is the constituent mass of the ith quark (antiquark), which can be written as follows:

$$\begin{aligned}
\mu_{12} &= \frac{m_1 m_2}{m_1 + m_2}, \quad \mu_{34} = \frac{m_3 m_4}{m_3 + m_4}, \quad \mu_{56} = \frac{m_5 m_6}{m_5 + m_6}, \\
\mu_{12,34} &= \frac{(m_1 + m_2)(m_3 + m_4)}{m_1 + m_2 + m_3 + m_4}, \\
\mu_{1234,56} &= \frac{(m_1 + m_2 + m_3 + m_4)(m_5 + m_6)}{m_1 + m_2 + m_3 + m_4 + m_5 + m_6}, \\
\vec{p}_{12} &= \frac{m_2\vec{p}_1 - m_1\vec{p}_2}{m_1 + m_2}, \qquad \vec{p}_{34} = \frac{m_4\vec{p}_3 - m_3\vec{p}_4}{m_3 + m_4}, \\
\vec{p}_{56} &= \frac{m_6\vec{p}_5 - m_5\vec{p}_6}{m_5 + m_6}, \\
\vec{p}_{12,34} &= \frac{(m_3 + m_4)\vec{p}_{12} - (m_1 + m_2)\vec{p}_{34}}{m_1 + m_2 + m_3 + m_4}, \\
\vec{p}_{1234,56} &= \frac{(m_1 + m_2 + m_3 + m_4)\vec{p}_{56} - (m_5 + m_6)\vec{p}_{1234}}{m_1 + m_2 + m_3 + m_4 + m_5 + m_6}.
\end{aligned} \quad (2)$$

In our investigation, we specifically consider dynamical chiral symmetry breaking [$V_{\chi,\chi=\pi,\eta,K,\sigma}(\mathbf{r}_{ij})$], color confinement [$V_{\rm con}(\mathbf{r}_{ij})$], and perturbative one-gluon exchange interactions [$V_{\rm oge}(\mathbf{r}_{ij})$], which correspond to fundamental properties of QCD in its low energy regime. Given the

three-meson system ($c\overline{q} - c\bar{q} - q\bar{s}(q\bar{c})$) with negative parity, both S-wave and D-wave motions are present within this system. As a result, the potential included in our Hamiltonian incorporates both tensor force potential $[V^T(\mathbf{r}_{ij})]$ and spin-orbit coupling potential $[V^{SO}(\mathbf{r}_{ij})]$.

$V_{\rm con}(\mathbf{r}_{ij})$ represents the confining potential, mirroring the essential "confinement" characteristic of QCD. Based on lattice regularized QCD findings, it has been established that multigluon exchanges yield an attractive potential that increases linearly with the distance between infinitely heavy quarks. Within the quark model, three distinct potential energy forms exist: square confinement [20], linear confinement [21], and exponential confinement [22] with a screening effect. Square confinement and linear confinement potentials share similarities, while the exponential confinement potential is notable for its screening effect at a higher energy region. Given our focus on the bound state problem, there exists minimal disparity among these three potential energies. Therefore, we adopt a square confinement potential in this article. The $V_{\rm con}(\mathbf{r}_{ij})$ comprises both the central force $V^C_{\rm con}(\mathbf{r}_{ij})$ and the spin-orbit force $V^{SO}_{\rm con}(\mathbf{r}_{ij})$:

$$\begin{aligned} V^C_{\rm con}(\mathbf{r}_{ij}) &= (-a_c r_{ij}^2 - \Delta)\boldsymbol{\lambda}_i^c \cdot \boldsymbol{\lambda}_j^c, \\ V^{SO}_{\rm con}(\mathbf{r}_{ij}) &= -\boldsymbol{\lambda}_i^c \cdot \boldsymbol{\lambda}_j^c \frac{a_c}{4m_i^2 m_j^2}[((m_i^2 + m_j^2)(1 - 2a_s) \\ &\quad + 4m_i m_j(1 - a_s))(\vec{S}_+ \cdot \vec{L}) \\ &\quad + ((m_j^2 - m_i^2)(1 - 2a_s))(\vec{S}_- \cdot \vec{L})]. \end{aligned} \tag{3}$$

TABLE I. Quark model parameters ($m_\pi = 0.7$ fm^{-1}, $m_\sigma = 3.42$ fm^{-1}, $m_\eta = 2.77$ fm^{-1}). There are two sets of chiral quark model parameters, the different parts of which are separated by /.

Quark masses	$m_u = m_d$ (MeV)	313
	m_s (MeV)	526/490
	m_c (MeV)	1728/1780
Goldstone bosons	Λ_π(fm^{-1})	4.2
	Λ_η(fm^{-1})	5.2
	$g^2_{\rm ch}/(4\pi)$	0.54
	$\theta_p(^\circ)$	−15
Confinement	a_c (MeV fm^{-2})	101
	Δ (MeV)	−78.3
OGE	α_{qq}	0.5723
	α_{qc}	0.4938/0.4865
	α_{qs}	0.5350/0.5106
	α_{cc}	0.3753
	$\hat{r}_0$ (MeV)	28.17
	$\hat{r}_g$ (MeV)	34.5
	a_s	0.777

In Eqs. (3), the parameters a_c, a_s, and Δ are defined and listed in Table I, and $\vec{S}_\pm = \vec{S}_i \pm \vec{S}_j$. $\boldsymbol{\lambda}^c$ are $SU(3)$ color Gell-Mann matrices.

Dynamical chiral symmetry breaking leads to the emergence of the Goldstone boson exchange interactions among constituent light quarks u, d, and s. The chiral part of the Hamiltonian $V_\chi(\mathbf{r}_{ij})$ can be resumed as follows:

$$V_\chi(\mathbf{r}_{ij}) = V^C_{\pi,\eta,K,\sigma}(\mathbf{r}_{ij}) + V^T_{\pi,\eta,K}(\mathbf{r}_{ij}) + V^{SO}_\sigma(\mathbf{r}_{ij}), \tag{4}$$

where C stands for central, T for tensor, and SO for spin-orbit potentials. The central part presents four different contributions,

$$V^C_\chi(\mathbf{r}_{ij}) = V^C_\pi(\mathbf{r}_{ij}) + V^C_K(\mathbf{r}_{ij}) + V^C_\eta(\mathbf{r}_{ij}) + V^C_\sigma(\mathbf{r}_{ij}), \tag{5}$$

where it can be written as follows:

$$\begin{aligned} V^C_\pi(\mathbf{r}_{ij}) &= \frac{g^2_{\rm ch}}{4\pi}\frac{m_\pi^2}{\Lambda_\pi^2 - m_\pi^2}\frac{\Lambda_\pi^2}{\Lambda_\pi^2 - m_\pi^2} m_\pi \Big[Y(m_\pi r_{ij}) \\ &\quad - \frac{\Lambda_\pi^3}{m_\pi^3} Y(\Lambda_\pi r_{ij})\Big](\vec{\sigma}_i \cdot \vec{\sigma}_j)\sum_{a=1}^{3} \boldsymbol{\lambda}_i^a \boldsymbol{\lambda}_j^a, \\ V^C_K(\mathbf{r}_{ij}) &= \frac{g^2_{\rm ch}}{4\pi}\frac{m_K^2}{\Lambda_K^2 - m_K^2}\frac{\Lambda_K^2}{\Lambda_K^2 - m_K^2} m_K \Big[Y(m_K r_{ij}) \\ &\quad - \frac{\Lambda_K^3}{m_K^3} Y(\Lambda_K r_{ij})\Big](\vec{\sigma}_i \cdot \vec{\sigma}_j)\sum_{a=4}^{7} \boldsymbol{\lambda}_i^a \boldsymbol{\lambda}_j^a, \\ V^C_\eta(\mathbf{r}_{ij}) &= \frac{g^2_{\rm ch}}{4\pi}\frac{m_\eta^2}{\Lambda_\eta^2 - m_\eta^2}\frac{\Lambda_\eta^2}{\Lambda_\eta^2 - m_\eta^2} m_\eta \Big[Y(m_\eta r_{ij}) \\ &\quad - \frac{\Lambda_\eta^3}{m_\eta^3} Y(\Lambda_\eta r_{ij})\Big](\vec{\sigma}_i \cdot \vec{\sigma}_j)\Big[\cos\theta_P(\boldsymbol{\lambda}_i^8 \boldsymbol{\lambda}_j^8) - \frac{2}{3}\sin\theta_P\Big], \\ V^C_\sigma(\mathbf{r}_{ij}) &= \frac{g^2_{\rm ch}}{4\pi}\frac{\Lambda_\sigma^2}{\Lambda_\sigma^2 - m_\sigma^2} m_\sigma \Big[Y(m_\sigma r_{ij}) - \frac{\Lambda_\sigma}{m_\sigma} Y(\Lambda_\sigma r_{ij})\Big], \end{aligned} \tag{6}$$

where $\boldsymbol{\lambda}^a$ are $SU(3)$ flavor Gell-Mann matrices, m_π and m_η are the masses of $SU(3)$ Goldstone bosons, taken to be their experimental values; m_σ is determined by the relation $m_\sigma^2 \approx m_\pi^2 + 4m_{u,d}^2$. Λ_χ is the cutoff, and $g^2_{\rm ch}/4\pi$ is the Goldstone-quark coupling constant, which is determined from the $NN\pi$ coupling constant. Finally, $Y(x)$ is the standard Yukawa function defined by $Y(x) = e^{-x}/x$, $G(x) = (1 + 1/x)Y(x)/x$, and $H(x) = (1 + 3/x + 3/x^2)Y(x)/x$.

There are three different contributions to the tensor potential

$$V^T_\chi(\mathbf{r}_{ij}) = V^T_\pi(\mathbf{r}_{ij}) + V^T_K(\mathbf{r}_{ij}) + V^T_\eta(\mathbf{r}_{ij}), \tag{7}$$

with each interaction given by

$$V_\pi^T(\mathbf{r}_{ij}) = \frac{g_{\rm ch}^2}{4\pi}\frac{m_\pi^2}{\Lambda_\pi^2 - m_\pi^2}\frac{\Lambda_\pi^2}{\Lambda_\pi^2 - m_\pi^2} m_\pi \left[H(m_\pi r_{ij}) - \frac{\Lambda_\pi^3}{m_\pi^3} H(\Lambda_\pi r_{ij})\right] S_{ij} \sum_{a=1}^{3} \boldsymbol{\lambda}_i^a \boldsymbol{\lambda}_j^a,$$

$$V_K^T(\mathbf{r}_{ij}) = \frac{g_{\rm ch}^2}{4\pi}\frac{m_K^2}{\Lambda_K^2 - m_K^2}\frac{\Lambda_K^2}{\Lambda_K^2 - m_K^2} m_K \left[H(m_K r_{ij}) - \frac{\Lambda_K^3}{m_K^3} H(\Lambda_K r_{ij})\right] S_{ij} \sum_{a=4}^{7} \boldsymbol{\lambda}_i^a \boldsymbol{\lambda}_j^a,$$

$$V_\eta^T(\mathbf{r}_{ij}) = \frac{g_{\rm ch}^2}{4\pi}\frac{m_\eta^2}{\Lambda_\eta^2 - m_\eta^2}\frac{\Lambda_\eta^2}{\Lambda_\eta^2 - m_\eta^2} m_\eta \left[H(m_\eta r_{ij}) - \frac{\Lambda_\eta^3}{m_\eta^3} H(\Lambda_\eta r_{ij})\right] S_{ij} \left[\cos\theta_P (\boldsymbol{\lambda}_i^8 \boldsymbol{\lambda}_j^8) - \frac{2}{3}\sin\theta_P\right], \quad (8)$$

where S_{ij} is defined by $3(\vec{\sigma}_i \cdot \hat{r}_{ij})(\vec{\sigma}_j \cdot \hat{r}_{ij}) - \vec{\sigma}_i \cdot \vec{\sigma}_j$. The spin-orbit potential solely arises from the scalar σ exchange between light quarks,

$$V_\sigma^{SO}(\mathbf{r}_{ij}) = -\frac{g_{\rm ch}^2}{4\pi}\frac{\Lambda_\sigma^2}{\Lambda_\sigma^2 - m_\sigma^2}\frac{m_\sigma^3}{2m_i m_j}\left[G(m_\sigma r_{ij}) - \frac{\Lambda_\sigma^3}{m_\sigma^3} G(\Lambda_\sigma r_{ij})\right] \vec{L} \cdot \vec{S}. \quad (9)$$

Beyond the scale of chiral symmetry breaking, one expects that the dynamics are influenced by QCD perturbative effects. These effects mimic gluon fluctuations around the instanton vacuum and are incorporated through the $V_{\rm OGE}(\mathbf{r}_{ij})$ which contains central force $V_{\rm oge}^C(r_{ij})$, spin-orbit force $V_{\rm oge}^{SO}(r_{ij})$, and tensor force $V_{\rm oge}^T(r_{ij})$. The central potential can be written as

$$V_{\rm oge}^C(r_{ij}) = \frac{\alpha_s}{4}\boldsymbol{\lambda}_i^c \cdot \boldsymbol{\lambda}_j^c \left[\frac{1}{r_{ij}} - \frac{2\pi}{3}\frac{\boldsymbol{\sigma}_i \cdot \boldsymbol{\sigma}_j}{m_i m_j}\delta(r_{ij})\right], \quad (10)$$

where $\boldsymbol{\sigma}$ are the $SU(2)$ Pauli matrices, $r_0(\mu_{ij}) = \frac{r_0}{\mu_{ij}}$, and α_s is an effective scale-dependent running coupling,

$$\alpha_s(\mu_{ij}) = \frac{\alpha_0}{\ln\left[(\mu_{ij}^2 + \mu_0^2)/\Lambda_0^2\right]}. \quad (11)$$

The $\delta(r_{ij})$ function, arising as a consequence of the nonrelativistic reduction of the one-gluon exchange diagram between pointlike particles, has to be regularized in order to perform exact calculations. It reads

$$\delta(\mathbf{r}_{ij}) = \frac{e^{-r_{ij}/r_0(\mu_{ij})}}{4\pi r_{ij} r_0^2(\mu_{ij})}.$$

The spin-orbit force $V_{\rm oge}^{SO}(r_{ij})$ and tensor force $V_{\rm oge}^T(r_{ij})$ can be written as

$$V_{\rm oge}^{SO}(r_{ij}) = -\frac{1}{16}\frac{\alpha_s \boldsymbol{\lambda}_i^c \cdot \boldsymbol{\lambda}_j^c}{4m_i^2 m_j^2}\left[\frac{1}{r_{ij}^3} - \frac{e^{-r_{ij}/r_g(\mu)}}{r_{ij}^3}\left(1 + \frac{r_{ij}}{r_g(\mu)}\right)\right] \times [(m_i^2 + m_j^2 + 4m_i m_j)(\vec{S}_+ \cdot \vec{L}) + (m_j^2 - m_i^2)(\vec{S}_- \cdot \vec{L})], \quad (12a)$$

$$V_{\rm oge}^T(r_{ij}) = -\frac{1}{16}\frac{\alpha_s \boldsymbol{\lambda}_i^c \cdot \boldsymbol{\lambda}_j^c}{4m_i^2 m_j^2}\left[\frac{1}{r_{ij}^3} - \frac{e^{-r_{ij}/r_g(\mu)}}{r_{ij}}\left(\frac{1}{r_{ij}^2} + \frac{1}{3r_g^2(\mu)} + \frac{1}{r_{ij} r_g(\mu)}\right)\right] S_{ij}. \quad (12b)$$

All the parameters are determined by fitting the meson spectrum, taking into account only a quark-antiquark component. They are shown in Table I.

III. THE WAVE FUNCTION

At the quark level, the six quarks are divided into three subclusters as shown in Fig. 1. In this case, q_1 and $\bar{q}_2$ form the first subcluster wave function $\psi(r)$; q_3 and $\bar{q}_4$ form the second subcluster wave function $\psi(R)$; q_5 and $\bar{q}_6$ form the third subcluster wave function $\psi(\xi)$; the wave function $\psi(\rho)$ represents the relative motion between the first subcluster and the second subcluster; the wave function $\psi(\lambda)$ represents the relative motion between one cluster composed of q_1, $\bar{q}_2$, q_3, and $\bar{q}_4$ and the third subcluster. The total wave function of a hexaquark system is the internal product of color, spin, flavor, and space wave functions of three subclusters and two spatial relative motions. The total wave function $\Psi_i(\mathbf{r})$ can be expanded as follows:

$$\Psi_{i,j,k}(\mathbf{r}) = \mathcal{A}\psi_i^{SO}(\mathbf{r})\chi^f\chi^c. \quad (13)$$

In Eq. (13), ψ_i^{SO} represents the function describing spin-orbit coupling, χ^f denotes the flavor wave function, and χ^c

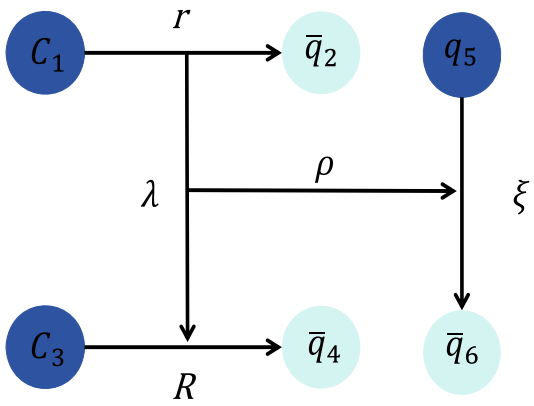

FIG. 1. The spatial configuration of D^*DK or $D^*D\bar{D}$.

represents the color wave function. $\mathcal{A}$ signifies the antisymmetrization operator. Since only two pairs of identical particles, namely c_1 and c_3, as well as q_2 and q_4, exist in the two systems under investigation, the expression for our antisymmetrization operator can be written as follows:

$$\mathcal{A} = 1 - (13) - (24) + (13)(24). \tag{14}$$

In the following section, we will briefly outline the process of obtaining each part of the wave function. First, we begin with the flavor wave function. Since we are studying the hexaquark system of T_{cc} partners, two flavor wave functions are obtained:

$$\chi^{f1} = \frac{1}{\sqrt{2}}(c\bar{u}c\bar{d}u\bar{c} - c\bar{d}c\bar{u}u\bar{c}) \tag{15}$$

for the $D^*D\bar{D}$ system and

$$\chi^{f2} = \frac{1}{\sqrt{2}}(c\bar{u}c\bar{d}u\bar{s} - c\bar{d}c\bar{u}u\bar{s}) \tag{16}$$

for the D^*DK system.

As we substitute the contribution of color-excited states with the $S-D$ coupling effects in this paper, for the total color wave function of the hexaquark of T_{cc} partners, we only consider the colorless wave function obtained by three coupled color-singlet clusters, $1 \otimes 1 \otimes 1$:

$$\chi^c = \frac{1}{\sqrt{3}}(\bar{r}r + \bar{g}g + \bar{b}b) \times \frac{1}{\sqrt{3}}(\bar{r}r + \bar{g}g + \bar{b}b) \times \frac{1}{\sqrt{3}}(\bar{r}r + \bar{g}g + \bar{b}b). \tag{17}$$

Since J is a good quantum number, we couple the spatial orbital wave functions $\psi_L(\mathbf{r})$ and spin wave function χ_S of the three subclusters to form $\psi_J(\mathbf{r})$; the specific details can be found in our previous work [23]. The $\psi_J(\mathbf{r})$ of these three subclusters can be expressed as follows:

$$\psi_{J_1,mJ_1}(r) = \phi_{L_1,mL_1}(r) \otimes \chi_{S_1,mS_1}, \tag{18}$$

$$\psi_{J_2,mJ_2}(R) = \phi_{L_2,mL_2}(R) \otimes \chi_{S_2,mS_2}, \tag{19}$$

$$\psi_{J_3,mJ_3}(\xi) = \phi_{L_3,mL_3}(\xi) \otimes \chi_{S_3,mS_3}. \tag{20}$$

The wave functions $\psi_{J_1,mJ_1}(r)$ of the first subcluster and $\psi_{J_2,mJ_2}(R)$ of the second subcluster are coupled to form the wave function $\psi_{J_{12}}$. Subsequently, this coupled wave function is coupled with the wave function $\psi_{J_3,mJ_3}(\xi)$ of the third subcluster to obtain the wave function $\psi_{J_{123}}$. Two relative motion wave functions $\phi_{L_4,mL_4}(\lambda)$ and $\phi_{L_5,mL_5}(\rho)$ are sequentially coupled with the wave function $\psi_{J_{123}}$ to finally obtain the total orbit-spin wave function $\psi_i^{SO}(\mathbf{r})$:

$$\psi_{J_{12},mJ_{12}} = \psi_{J_1,mJ_1}(\boldsymbol{r}) \otimes \psi_{J_2,mJ_2}(\boldsymbol{R}), \tag{21}$$

$$\psi_{J_{123},mJ_{123}} = \psi_{J_{12},mJ_{12}} \otimes \psi_{J_3,mJ_3}(\boldsymbol{\xi}), \tag{22}$$

$$\psi_{JL_4,mJL_4} = \psi_{J_{123},mJ_{123}} \otimes \psi_{L_4,mL_4}(\boldsymbol{\lambda}), \tag{23}$$

$$\psi_i^{SO}(\boldsymbol{r}) = \psi_{JL_4,mJL_4} \otimes \phi_{L_5,mL_5}(\boldsymbol{\rho}), \quad i \equiv \{L_1, S_1, J_1, L_2, S_2, J_2, L_3, S_3, J_3, J_{12}, J_{123}, JL_4, L_4, L_5\}. \tag{24}$$

During this coupling process, a total of 14 variables are involved, denoted simply as combinations represented by the index i. Given that our calculation focuses on the bound states of the hexaquark system of T_{cc} partners, all three subclusters are in the ground state. Additionally, J_{12}, J_{123}, and JL_4 are all set to 1. Their intercluster motion can be either S-wave or D-wave. We have listed their possible combinations in Table II. Because of no difference between the spins of quark and antiquark, the meson-meson structure has the same spin wave function as the diquark-antidiquark structure. The spin wave functions of the subcluster are shown below,

$$\chi_\sigma^{11} = \alpha\alpha, \qquad \chi_\sigma^{10} = \frac{1}{\sqrt{2}}(\alpha\beta + \beta\alpha),$$
$$\chi_\sigma^{1-1} = \beta\beta, \qquad \chi_\sigma^{00} = \frac{1}{\sqrt{2}}(\alpha\beta - \beta\alpha).$$

In the context of quark spin, α and β represent the third component of the quark spin, taking values of $\frac{1}{2}$ and $-\frac{1}{2}$, respectively, in two distinct cases.

Finally, the spatial wave functions are Gaussians with range parameters chosen to lie in a geometrical progression:

$$\phi_{nLm}(\mathbf{r}) = N_{nL} r^L e^{-(r/r_n)^2} Y_{Lm}(\hat{r}), \tag{25}$$

TABLE II. Different combinations of $J-J$ coupling.

$J_1 = 0$		$J_2 = 1$		$J_3 = 0$			i
$L_1 = 0$	$S_1 = 0$	$L_2 = 0$	$S_2 = 1$	$L_3 = 0$	$S_3 = 0$	$L_4 = 0$	1
$L_1 = 0$	$S_1 = 0$	$L_2 = 0$	$S_2 = 1$	$L_3 = 0$	$S_3 = 1$	$L_4 = 2$	2
$J_1 = 1$		$J_2 = 1$		$J_3 = 0$			i
$L_1 = 0$	$S_1 = 1$	$L_2 = 0$	$S_2 = 1$	$L_3 = 0$	$S_3 = 0$	$L_4 = 0$	3
$L_1 = 0$	$S_1 = 1$	$L_2 = 0$	$S_2 = 1$	$L_3 = 0$	$S_3 = 1$	$L_4 = 2$	4

TABLE III. Results of calculations for the D^*DK and $DD^*\bar{D}$ systems. The first and second lines represent the results of the S-wave $DD^*K(\bar{D})$ and $D^*D^*K(\bar{D})$, respectively, while the third and fourth lines represent the results of the D-wave $DD^*K(\bar{D})$ and $D^*D^*K(\bar{D})$. $c.c.1$ and $B.E.1$ denote the channel couplings and binding energies under the S-wave configuration, while $c.c.2$ and $B.E.2$ denote the channel couplings and binding energies under the combined S-wave and D-wave configurations. The calculation error comes from the difference between the results of the two sets of parameters and the average values of the two sets of parameters. (Unit: MeV.).

Index	Channel	E	Channel	E
1	S-wave-DD^*K	4365.2	S-wave-$DD^*\bar{D}$	5736.4
2	S-wave-D^*D^*K	4507.2	S-wave-$D^*D^*\bar{D}$	5878.4
3	D-wave-DD^*K	4368.3	D-wave-$DD^*\bar{D}$	5738.5
4	D-wave-D^*D^*K	4509.5	D-wave-$D^*D^*\bar{D}$	5880.6
$c.c.1$		4364.9 ± 0.3		5735.3 ± 0.2
$B.E.1$		$-(0.3 \pm 0.3)$		$-(1.1 \pm 0.2)$
$c.c.2$		4364.8 ± 0.4		5734.8 ± 0.3
$B.E.2$		$-(0.4 \pm 0.4)$		$-(1.6 \pm 0.3)$

where N_{nL} are normalization constants, which can be expressed by a general formula

$$N_{nL} = \left[\frac{2^{L+2}(2\nu_n)^{L+\frac{3}{2}}}{\sqrt{\pi}(2L+1)!!}\right]^{\frac{1}{2}}. \tag{26}$$

IV. RESULTS AND DISCUSSIONS

In this work, we primarily investigate the possibility of bound states $D^*D\bar{D}$ and D^*DK. Because we are more concerned about the binding energy magnitude and also want to ensure comparison with experimental results, we apply a mass correction to the theoretical computed results, where the final energy is the experimental threshold plus the bounding energy ($E = \text{Threshold}_{\text{EXP.}} + B.E.$). To reduce the dependence of our computational results on model parameters, we adjusted two sets of parameters for bound state calculations. The average of these results is taken as the central value, while the discrepancy between the two sets of calculations determines the upper and lower limits of the error [E(average value) $\pm$ error].

D^*DK sector: Taking into account $IJ^P = 01^-$, in the hexaquark system $c\bar{q}c\bar{q}q\bar{s}$, we have considered four physical channels: D^*DK, D^*D^*K, as well as D-wave-D^*DK and D-wave-D^*D^*K. The results of our calculations for these channels are presented in Table III. The energies of these four channels are about 4.4 GeV, and none of them are bound states. However, when we consider the coupling effects of the S-wave D^*DK and D^*D^*K channels, the coupling effect lowers the energy of the D^*DK channel, which was relatively lower, below the threshold line by 0.3 ± 0.3 MeV. Subsequently, we additionally consider the coupling effect of $S-D$, and the results show that the binding energy further increases to 0.4 ± 0.4 MeV. To understand the binding mechanism of D^*DK, we calculated the contributions of each term in the Hamiltonian to the binding energy (the contribution of each potential energy term of the coupling energy minus the contribution of each potential energy term of the threshold channels) as well as the root-mean-square (rms) distance. The results are presented in Table IV. The results indicate that the kinetic energy is repulsive, while most of the other potential energy terms are attractive, with the color-magnetic term, π-meson exchange, and σ-meson exchange playing a major role. This is attributed to the relatively large spacing between quarks, resulting in long-range attraction dominating the potential energy. It is worth noting that the binding energy of the D^*DK system is generally small overall. Under the second set of parameters, the D^*DK system is unbound. Based on the rms calculation, we further plotted the spatial structure of the bound state D^*DK, as shown in Fig. 2(a). We denote the quarks in the $c\bar{q}c\bar{q}q\bar{s}$ system as 1, 2, 3, 4, 5, and 6. Due to the identical nature of particles c_1 and c_3, as well as $\bar{q}_2$ and $\bar{q}_4$, we obtain $r_{c_1\bar{q}_2} = r_{c_1\bar{q}_4} = r_{\bar{q}_2c_3} = r_{c_3\bar{q}_4}$. However, these values do not represent the true distances between particles but rather an averaged effect. Using a triangular approximation [$r^2_{c_1\bar{q}_2} = (r^2_{\text{re}} + r^2_{\bar{q}_2\bar{q}_4})/2$], where

TABLE IV. The root-mean-square distances (unit: fm) and contributions of all potentials to the binding energy (unit: MeV) in D^*DK and $D^*D^*\bar{D}$ systems. The calculation error comes from the difference between the results of the two sets of parameters and the average values of the two sets of parameters. Where, "q" represents the "u" and "d" quarks, while "Q'" denotes the "$\bar{c}$" (or "$\bar{s}$") quark.

	Kinetic	Confinement	Cl.	C.m.	π	η	σ	$r_{c\bar{q}}$	r_{cq}	$r_{cQ'}$	$r_{q\bar{q}}$	$r_{Q'\bar{q}}$	$r_{Q'q}$
D^*DK	32.7 ± 0.7	$-(1.7 \pm 0.1)$	$-(2.0 \pm 0.1)$	$-(9.3 \pm 0.2)$	$-(12.8 \pm 0.2)$	0.1 ± 0.1	$-(7.0 \pm 0.2)$	1.7	5.5	2.3	2.4	5.5	0.6
$D^*D\bar{D}$	28.9 ± 1.1	$-(1.5 \pm 0.1)$	$-(1.7 \pm 0.1)$	$-(7.5 \pm 0.4)$	$-(12.4 \pm 0.4)$	0.4 ± 0.1	$-(7.7 \pm 0.3)$	1.7	4.9	2.3	2.4	4.9	0.6

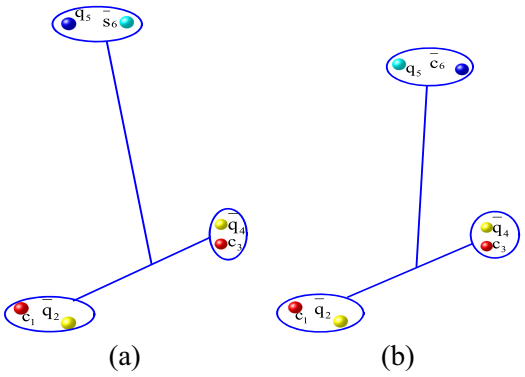

FIG. 2. (a) DD^*K spatial structure, (b) $DD^*\bar{D}$ spatial structure.

r_{re} is the real rms of $r_{c_1\bar{q}_2}$, we can obtain a cluster of one meson $(c-\bar{q})$ with a distance of about 0.54 fm, which is close to the rms we calculated for this meson alone. Overall, the distance between two quarks from different clumps is larger than 2 fm but the rms within the same cluster is about 0.5 fm, suggesting that the two clumps are separated by a wide distance. In Fig. 2(a), we can see that the first two mesons (D^*D) are relatively compact, while the third meson K is slightly farther away from the first two. The overall structure resembles that of a nucleon-electron system.

$D^*D\bar{D}$ sector: Similar to the $c\bar{q}c\bar{q}q\bar{s}$ system, in the $c\bar{q}c\bar{q}q\bar{c}$ system, we considered four physical channels: $D^*D\bar{D}$, $D^*D^*\bar{D}$, as well as D-wave-$D^*D\bar{D}$ and D-wave-$D^*D^*\bar{D}$. The bound state calculations show that these four single channels are all scattering states. The coupling energy of the two physical channels $D^*D\bar{D}$ and $D^*D^*\bar{D}$, both in the S-wave, is 5735.3 ± 0.2 MeV, and their binding energy is 0.9 ± 0.4 MeV. The binding energy obtained by the coupling of these two channels is already deeper than the binding energy of the four channels in the $c\bar{q}c\bar{q}q\bar{s}$ system. Then, we considered the contribution of the D-wave to the final binding energy. The calculation results show that the coupling effect of the D-wave increases the binding energy by an additional 0.5 MeV, resulting in a total binding energy of 1.6 ± 0.3 MeV. Compared to the $c\bar{q}c\bar{q}q\bar{s}$ system, the quarks in the third cluster of the $c\bar{q}c\bar{q}q\bar{c}$ system are heavier, so although their kinetic energy is also repulsive, it is slightly lower than that of the former. This conclusion is supported by the root-mean-square distance of $D^*D^*\bar{D}$ in Table IV, where the third subcluster is closer to the first two subclusters, as shown in Fig. 2(b).

V. SUMMARY

Inspired by the discovery of T_{cc} (D^*D) experimentally, we combined two other well-known states, $X(3872)$ $(D^*\bar{D})$ and $D_{s0}^*(2317)$ (DK), to construct two hexaquark systems, D^*DK and $D^*D\bar{D}$. At the quark level, utilizing the Gaussian expansion method, we performed dynamical studies on these two systems.

The calculated results reveal that both systems exhibit bound states, with the binding energy of D^*DK slightly smaller than that of $D^*D\bar{D}$. Due to the similarity in quark composition between these two systems, the contributions of various terms in the Hamiltonian to their binding energies are quite similar, primarily dominated by long-range potential energy attraction and kinetic energy repulsion. The calculation of the root-mean-square distance allowed us to depict the spatial structures of these two systems, resembling that of a nucleon-electron system. As the third meson D in $D^*D\bar{D}$ is significantly heavier than the third meson K in D^*DK, the spatial structure of the $D^*D\bar{D}$ system is more compact, with slightly less kinetic energy repulsion compared to the D^*DK system.

Considering the complexity of six-quark calculations, we only considered four physical channels in each system. If more excited states, such as P-wave and D-wave, are taken into account, perhaps the binding energies of these two systems would be deeper. However, the fact that the D^*DK and $D^*D\bar{D}$ systems form bound states with only two channels coupled indicates their stability, strongly suggesting further experimental exploration in the future.

ACKNOWLEDGMENTS

This work is supported partly by the National Natural Science Foundation of China under Grants No. 12205249, No. 12205125, No. 11865019, No. 11775118, and No. 11535005 by the Natural Science Foundation of Jiangsu Province (BK20221166), the Science and Technology Foundation of Bijie (Grant No. BiKeLianHe [2023]17), and the Funding for School-Level Research Projects of Yancheng Institute of Technology (No. xjr2022039).

[1] S. K. Choi *et al.* (Belle Collaboration), Phys. Rev. Lett. **91**, 262001 (2003).
[2] S. Godfrey and N. Isgur, Phys. Rev. D **32**, 189 (1985).
[3] E. S. Swanson, Phys. Lett. B **598**, 197 (2004).
[4] N. A. Tornqvist, Phys. Lett. B **590**, 209 (2003).
[5] Y. Yang and J. Ping, Phys. Rev. D **81**, 114025 (2010).
[6] Y. Yang, J. Ping, C. Deng, and H. S. Zong, J. Phys. G **39**, 105001 (2012).

[7] J. R. Zhang, Phys. Rev. D **87**, 116004 (2013).
[8] W. Qin, S. R. Xue, and Q. Zhao, J. Conf. Proc. **13**, 020022 (2017).
[9] R. Aaij *et al.* (LHCb Collaboration), Nat. Commun. **13**, 3351 (2022).
[10] N. V. Shevchenko and J. Haidenbauer, Phys. Rev. C **92**, 044001 (2015).
[11] A. Martinez Torres, K. P. Khemchandani, and L. S. Geng, Phys. Rev. D **99**, 076017 (2019).
[12] T. W. Wu, M. Z. Liu, L. S. Geng, E. Hiyama, and M. P. Valderrama, Phys. Rev. D **100**, 034029 (2019).
[13] Y. Huang, M. Z. Liu, Y. W. Pan, L. S. Geng, A. Martínez Torres, and K. P. Khemchandani, Phys. Rev. D **101**, 014022 (2020).
[14] Y. W. Pan, T. W. Wu, M. Z. Liu, and L. S. Geng, Phys. Rev. D **105**, 114048 (2022).
[15] Q. H. Shen, X. Zhang, X. Liu, and J. J. Xie, Phys. Rev. D **109**, 014012 (2024).
[16] P. G. Ortega, arXiv:2403.10244.
[17] T. C. Wu and L. S. Geng, Phys. Rev. D **108**, 014015 (2023).
[18] M. C. Gordillo and J. Segovia, Phys. Rev. D **109**, 094032 (2024).
[19] S. P. Jin and H. Y. Jiang, arXiv:2403.13087.
[20] Y. Tan, W. Lu, and J. Ping, Eur. Phys. J. Plus **135**, 716 (2020).
[21] G. Yang, J. Ping, and J. Segovia, Phys. Rev. D **104**, 014006 (2021).
[22] J. Vijande, F. Fernandez, and A. Valcarce, J. Phys. G **31**, 481 (2005).
[23] Y. Tan, X. Liu, X. Chen, Y. Wu, H. Huang, and J. Ping, Phys. Rev. D **109**, 076026 (2024).